Article

Solar Neutrinos Spectroscopy with Borexino Phase-II

L. Miramonti [10,*] on behalf of the Borexino Collaboration,

M. Agostini [17,] **K. Altenmüller** [17,] **S. Appel** [17,] **V. Atroshchenko** [7,] **Z. Bagdasarian** [24,] **D. Basilico** [10,]
G. Bellini [10,] **J. Benziger** [14,] **D. Bick** [4,] **I. Bolognino** [10,] **G. Bonfini** [9,] **D. Bravo** [10,] **B. Caccianiga** [10,]
F. Calaprice [13,] **A. Caminata** [3,] **S. Caprioli** [10,] **M. Carlini** [9,] **P. Cavalcante** [16,9,] **F. Cavanna** [3,]
A. Chepurnov [18,] **K. Choi** [23,] **L. Collica** [10,] **S. Davini** [3,] **A. Derbin** [12,] **X.F. Ding** [9,] **A. Di Ludovico** [13,]
L. Di Noto [3,] **I. Drachnev** [19,12,] **K. Fomenko** [2,] **A. Formozov** [2,] **D. Franco** [1,] **F. Gabriele** [9,] **C. Galbiati**
[13,] **M. Gschwender** [25,] **C. Ghiano** [9,] **M. Giammarchi** [10,] **A. Goretti** [13,] **M. Gromov** [18,] **D. Guffanti** [19,9,]
C. Hagner [4,] **T. Houdy** [1,] **E. Hungerford** [20,] **Aldo Ianni** [9,] **Andrea Ianni** [13,] **A. Jany** [5,] **D. Jeschke** [17,]
V. Kobychev [6,] **D. Korablev** [20,] **G. Korga** [2,] **T. Lachenmaier** [25,] **M. Laubenstein** [9,] **E. Litvinovich** [7,8,]
F. Lombardi [9,] **P. Lombardi** [10,] **L. Ludhova** [24,] **G. Lukyanchenko** [7,] **L. Lukyanchenko** [7,] **I. Machulin**
[7,8,] **G. Manuzio** [3,] **S. Marcocci** [19,] **J. Maricic** [23,] **J. Martyn** [22,] **E. Meroni** [10,] **M. Meyer** [21,] **M. Misiaszek**
[5,] **V. Muratova** [12,] **B. Neumair** [17,] **L. Oberauer** [17,] **B. Opitz** [4,] **V. Orekhov** [7,] **F. Ortica** [11,] **M. Pallavicini**
[3,] **L. Papp** [17,] **O. Penek** [24,] **L. Pietrofaccia** [9,] **N. Pilipenko** [12,] **A. Pocar** [15,] **A. Porcelli** [22,] **G. Raikov** [7,]
G. Ranucci [10,] **A. Razeto** [9,] **A. Re** [10,] **M. Redchuk** [24,] **A. Romani** [11,] **N. Rossi** [9,] **S. Rottenanger** [25,]
S. Schönert [17,] **D. Semenov** [12,] **M. Skorokhvatov** [7,8,] **O. Smirnov** [2,] **A. Sotnikov** [2,] **L.F.F. Stokes** [9,]
Y. Suvorov [9,7,] **R. Tartaglia** [9,] **G. Testera** [3,] **J. Thurn** [21,] **M. Toropova** [7,] **E. Unzhakov** [12,] **A. Vishneva** [2,]
R.B. Vogelaar [16,] **F. von Feilitzsch** [17,] **S. Weinz** [22,] **M. Wojcik** [5,] **M. Wurm** [22,] **Z. Yokley** [16,]
O. Zaimidoroga [2,] **S. Zavatarelli** [3,] **K. Zuber** [21,] **G. Zuzel** [5,]

[1]   AstroParticule et Cosmologie, Université Paris Diderot, CNRS/IN2P3, CEA/IRFU, Observatoire de Paris, Sorbonne Paris Cité, 75205 Paris Cedex 13, France
[2]   Joint Institute for Nuclear Research, 141980 Dubna, Russia
[3]   Dipartimento di Fisica, Università degli Studi e INFN, 16146 Genova, Italy
[4]   Institut für Experimentalphysik, Universität Hamburg, 22761 Hamburg, Germany
[5]   M. Smoluchowski Institute of Physics, Jagiellonian University, 30348 Krakow, Poland
[6]   Kiev Institute for Nuclear Research, 03680 Kiev, Ukraine
[7]   National Research Centre Kurchatov Institute, 123182 Moscow, Russia
[8]   National Research Nuclear University MEPhI (Moscow Engineering Physics Institute), 115409 Moscow, Russia
[9]   INFN Laboratori Nazionali del Gran Sasso, 67010 Assergi (AQ), Italy
[10] Dipartimento di Fisica, Università degli Studi e INFN, 20133 Milano, Italy
[11] Dipartimento di Chimica, Biologia e Biotecnologie, Università degli Studi e INFN, 06123 Perugia, Italy
[12] St. Petersburg Nuclear Physics Institute NRC Kurchatov Institute, 188350 Gatchina, Russia
[13] Physics Department, Princeton University, Princeton, NJ 08544, USA
[14] Chemical Engineering Department, Princeton University, Princeton, NJ 08544, USA
[15] Amherst Center for Fundamental Interactions and Physics Department, University of Massachusetts, Amherst, MA 01003, USA
[16] Physics Department, Virginia Polytechnic Institute and State University, Blacksburg, VA 24061, USA
[17] Physik-Department and Excellence Cluster Universe, Technische Universität München, 85748 Garching, Germany
[18] Lomonosov Moscow State University Skobeltsyn Institute of Nuclear Physics, 119234 Moscow, Russia
[19] Gran Sasso Science Institute, 67100 L'Aquila, Italy
[20] Department of Physics, University of Houston, Houston, TX 77204, USA
[21] Department of Physics, Technische Universität Dresden, 01062 Dresden, Germany
[22] Institute of Physics and Excellence Cluster PRISMA, Johannes Gutenberg-Universität Mainz, 55099 Mainz, Germany
[23] Department of Physics and Astronomy, University of Hawaii, Honolulu, HI 96822, USA
[24] Institut für Kernphysik, Forschungszentrum Jülich, 52425 Jülich, Germany
[25] Kepler Center for Astro and Particle Physics, Universität Tübingen, 72076 Tübingen, Germany

*   Correspondence: lino.miramonti@mi.infn.it; Tel.: +39-025031304

Abstract: Solar neutrinos have played a central role in the discovery of the neutrino oscillation mechanism. They still are proving to be a unique tool to help investigate the fusion reactions that power stars and further probe basic neutrino properties. The Borexino neutrino observatory has been operationally acquiring data at Laboratori Nazionali del Gran Sasso in Italy since 2007. Its main goal is the real-time study of low energy neutrinos (solar or originated elsewhere, such as geo-neutrinos). The latest analysis of experimental data, taken during the so-called Borexino Phase-II (2011-present), will be showcased in this talk - yielding new high-precision, simultaneous wide band flux measurements of the four main solar neutrino components belonging to the "pp" fusion chain (pp, pep, ^{7}Be, ^{8}B), as well as upper limits on the remaining two solar neutrino fluxes (CNO and hep).

Keywords: Solar neutrinos; neutrino oscillation; Borexino.

1. Solar neutrinos production and detection

Electron neutrinos (ν_e) are copiously produced in stars by thermonuclear fusion of protons. Solar neutrinos emitted by our star provide a direct and unique tool to infer properties of the interior of the Sun. The main contribution to the solar luminosity comes from reactions belonging to the pp chain that account for $\sim$99% while the remaining $\sim$1% is due to the CNO cycle. In the Sun the CNO cycle plays a sub-dominant role but it becomes dominant in massive stars [1,2]. The effort to develop a model able to reproduce accurately the physical characteristics of the Sun, the spectra and the fluxes of the produced neutrino components, was initiated by John Bahcall in the mid-1960s. This model in now called the Standard Solar Model (SSM) [3]. Figure 1 shows the *pp* chain with the relative branching percentages and the CNO bi-cycle; the corresponding neutrino fluxes are plotted in figure 2. The spectrum is dominated by the low-energy ν_es coming from the *pp* reaction, and extend up to $\sim$18.8 MeV, the maximum energy reached by the *hep* neutrinos. Beside the continuous spectra there are two mono-energetic lines from ^{7}Be ν's (E$_\nu$ = 0.384 MeV with a BR of $\sim$10% and 0.862 MeV with a BR of $\sim$90%) and one mono-energetic line from *pep* ν's (E$_\nu$ = 1.44 MeV). Neutrinos emitted from the CNO cycle are expected to have a continuous energy spectrum extending up to 1.74 MeV.
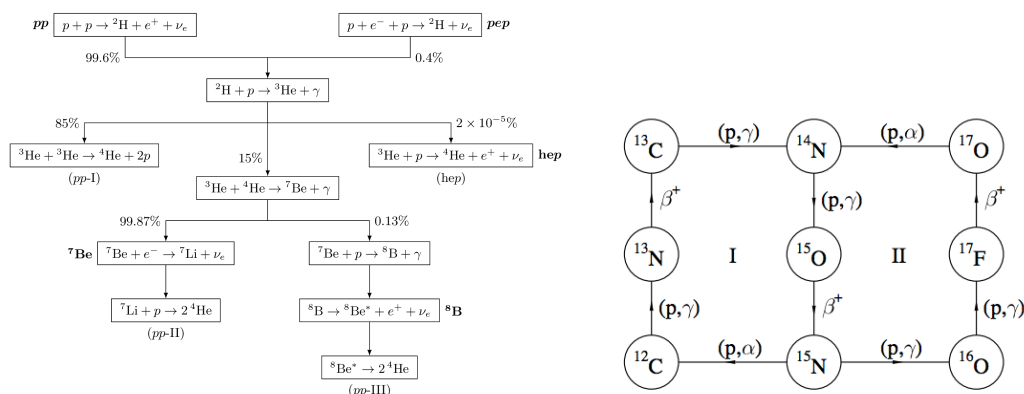

Figure 1. On the left frame the three principal cycles comprising the pp chain (ppI, ppII, and ppIII), with branching percentages indicated. On the right frame is shown the CNO bi-cycle. The CN cycle, marked I, produces $\sim$1% of solar energy and significant fluxes of solar neutrinos

In the last years, previous excellent agreement between the SSM and helioseismology (that is, the science that studies the interior of the Sun by looking at its vibration modes) has been seriously
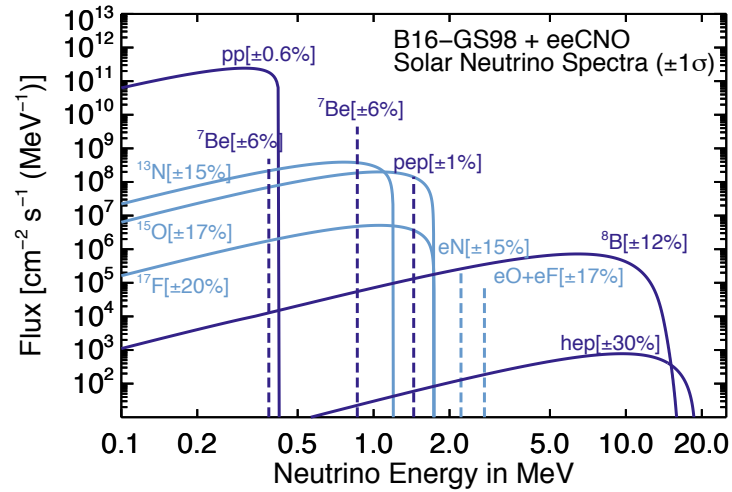
Figure 2. Neutrino fluxes form the pp chain and the CNO bi-cycle. Figure from [4]
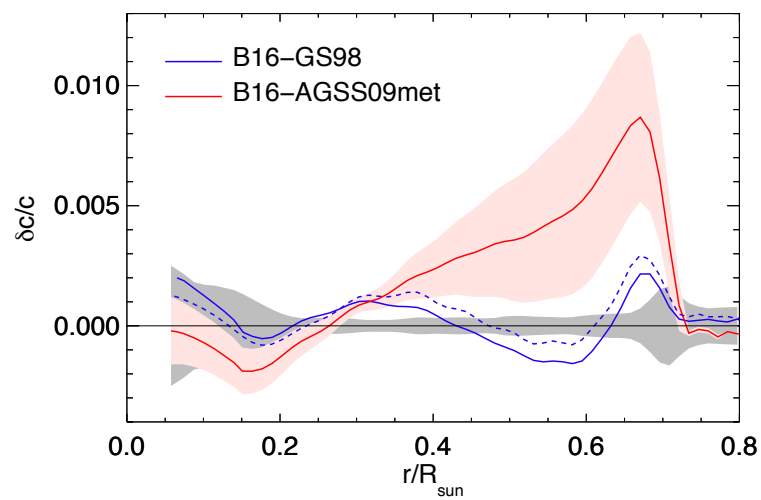

Figure 3. Fractional sound speed difference in the sense $\delta c/c = (c_\odot - c_{mod})/c_{mod}$. In blue the high metallicity and in red the low metallicity. Figure from [4]

compromised due to a downward revision of the heavy-element content at the solar surface from (Z/X) = 0.0229 [5] to (Z/X) = 0.0165 [6]. This profound discrepancy between the SSM and helioseismology is now called the Solar Metallicity Problem (see figure 3). To fix this puzzle would imply either to revise the physical inputs of the SSM or to modify the core abundances, in particular those of C,N,O.

A completely new revision of the abundances of almost all elements in the solar photosphere with a three-dimensional hydrodynamical model has been done in 2009 [7]. The new results gave a solar abundance (Z/X) = 0.0178. The three different sets (GS98 [5], AGS05 [6] and AGSS09 [7]) of solar abundances have been used in [8] originating two main different SSM variants: the low metallicity and the high metallicity SSMs.

In order to settle the low (LZ) versus high (HZ) metallicity problem it is important to experimentally measure the ^{7}Be, ^{8}B or CNO neutrino fluxes, which are sensitive to the solar metallicity. The difference between the two metallicities is ∼9% for ^{7}Be, ∼18% for ^{8}B and almost 40% for CNO (see table 1) [4].

Table 1. Model and solar neutrino fluxes. Units are: 10^{10} (pp), 10^9 (^{7}Be), 10^8 (pep, ^{13}N, ^{15}O), 10^6 (^{8}B,^{17}F) and 10^3(hep) cm^{-2}s^{-1}. Table adopted from [4]

Flux	B16-GS98	B16-AGSS09met
Φ(pp)	$5.98(1 \pm 0.006)$	$6.03(1 \pm 0.005)$
Φ(pep)	$1.44(1 \pm 0.01)$	$1.46(1 \pm 0.009)$
Φ(hep)	$7.98(1 \pm 0.30)$	$8.25(1 \pm 0.30)$
Φ(^{7}Be)	$4.93(1 \pm 0.06)$	$4.50(1 \pm 0.06)$
Φ(^{8}B)	$5.46(1 \pm 0.12)$	$4.50(1 \pm 0.12)$
Φ(^{13}N)	$2.78(1 \pm 0.15)$	$2.04(1 \pm 0.14)$
Φ(^{15}O)	$2.05(1 \pm 0.17)$	$1.44(1 \pm 0.16)$
Φ(^{17}F)	$5.29(1 \pm 0.20)$	$3.26(1 \pm 0.18)$

The first solar neutrino detector was built at the end of the 1960s in the Homestake mine in South Dakota in order to confirm the SSM. The deficit in detected neutrinos, about one third compared to the expected value form the SSM, was the start of the so called Solar Neutrino Problem (SNP) [9–12].

The detector consisted of a large tank filled with 615 metric tonnes of liquid perchloroethylene C_2Cl_4, suitable to detect ^{7}Be and ^{8}B νs, and a small signal from the CNO and *pep* solar neutrinos, via the reaction $\nu_e + {}^{37}Cl \rightarrow {}^{37}Ar + e^-$ with an energy threshold of $E_{th} = 814$ keV.

At the beginning of the 1980s Kamiokande, a large water Čerenkov detector of about 3000 metric tonnes, was built in Japan [13]. Kamiokande was a real time solar neutrino detector looking for the Čerenkov light produced by the electrons scattered by an impinging neutrino, mainly via the reaction $\nu_x + e^- \rightarrow \nu_x + e^-$. The energy threshold of the reaction was $E_{th} = 7.5$ MeV and, therefore, only ^{8}B and *hep* neutrinos were detected. At the beginning of the '90s a larger version of the detector was built, Super-Kamiokande, a 50000 metric tonne pure water detector with the energy threshold lowered to $E_{th} = 5.5$ MeV [14]. Both Kamiokande and Super-Kamiokande detected about half of the neutrinos foreseen by the SSM.

The SNP was also confirmed by two new radiochemical experiments with a very low energy threshold of $E_{th} = 233$ keV, via the reaction $\nu_e + {}^{71}Ga \rightarrow {}^{71}Ge + e^-$. The Soviet-American Gallium Experiment (SAGE), used more than 50 metric tons of metallic gallium [15], while the Gallex experiment at the Gran Sasso Underground Laboratories (LNGS), employed 30 metric tonnes of natural gallium [16,17]. Both detectors were calibrated with an artificial neutrino source. They looked for a less model-dependent component of neutrino spectra and hence more robust to test the hypothesis that fusion of hydrogen powers the Sun. Both experiments measured a smaller neutrino signal, by about 60%, than predicted by the SSM (for an historical introduction see for instance [18]).

At the turn of the century, the advent of the heavy water-based Sudbury Neutrino Observatory (SNO) experiment was able to measure simultaneously three different interaction channels; the elastic scattering $\nu_x + e^- \rightarrow \nu_x + e^-$, the charged current $\nu_e + d \rightarrow e^- + p^+ + p^+$, that is sensitive only to electronic neutrinos and the neutral current $\nu_x + d \rightarrow \nu_x + p^+ + n$, receiving contributions from

all active flavors. SNO proved that the measured total neutrino flux detected via neutral current interactions was in good agreement with the theoretical predictions of the SSM. Only a fraction of these neutrinos had conserved their flavor during their travel from the core of the Sun to the Earth [19–21].

The two oscillation parameters that lead solar neutrino oscillations are Δm_{12}^2 and θ_{12} of the PMNS mixing matrix. Up to few MeV, the ν_e survival probabilities are described by vacuum oscillations, but at energies above some MeV, matter effects enhance the conversion $\nu_e \rightarrow \nu_{\mu,\tau}$, leading to a further suppression of the ν_e rate detected on Earth. This matter enhancement effect was first proposed by Wolfenstein and then reprised by Mikheyev and Smirnov, it is now called MSW effect [22,23]. It consists in the transformation of one neutrino species (flavor) into another one in a medium with varying density. This effect depends on the refraction of neutrinos in matter, the resonance and the adiabaticity and it is described in terms of the flavors and the relative phases of eigenstates and the transitions between eigenstates. The Large Mixing Angle (LMA) MSW effect provides the solution of the long standing Solar Neutrino Problem. The MSW-LMA oscillation scenario is confirmed by all the solar neutrino experiments both for vacuum and matter-dominated regimes. The vacuum-matter transition region ($\sim$from 1 to $\sim$5 MeV), however, remains to be explored and might hold evidence for non-standard neutrino interactions (NSI).

2. Borexino detector

In order to explore the whole neutrino spectrum it has been necessary to build a real time detector with an energy threshold as low as possible. The Borexino experiment was conceived mainly to detect the mono-energetic beryllium line, but it succeeded in measuring all the solar neutrino components from the *pp* cycle.

The Borexino detector is located at the Gran Sasso National Laboratories (LNGS) in central Italy, at a depth of $\sim$ 1.4 km of rock, equivalent to 3800 m of water. The flux of cosmic muons which cross the rock shielding and reach the underground halls is $\sim$ 1.2 $\mu\ m^{-2}h^{-1}$. Figure 4 shows a 3D sketch of the detector [24].

The active mass is composed by 278 tonnes of pseudocumene which is doped with 1.5 g/l of PPO, in order to enhance the scintillator properties, and it is contained in an 8.5 m diameter nylon Inner Vessel with a thickness of 125 μm. The Inner Vessel is surrounded by two concentric pseudocumene buffers doped with a light quencher (DMP). A Stainless Steel Sphere with a diameter of 13.7 m contains the scintillator and buffers. In turn this sphere is enclosed in a dome-shaped Water Tank containing 2100 tons of ultra-pure water as an additional shield.

The light created by the scintillator is detected by 2212 8" PhotoMultiplier Tubes (PMTs) distributed on the inner surface of the Stainless Steel Sphere. Into the Water Tank 208 8" PMTs detect the Čerenkov light radiated by cosmic muons. The principle of neutrino detection is based on elastic scattering on electrons in the target material $\nu_x + e^- \rightarrow \nu_x + e^-$.

The light yield of the scintillator is $\sim$10^4 photons per MeV, corresponding to $\sim$500 detected photoelectrons per MeV. The fast time response of $\sim$3 ns allows the reconstruction of the events' position by means of a time-of-flight technique; the precision in position reconstruction is within $\sim$10 cm at 1 MeV. Thanks to the position reconstruction it is possible to define a fiducial volume between 75 and 150 tonnes depending on the analysis type.

The light created by the scattered electron is emitted isotropically; thus it is impossible to distinguish the light generated by the signal from the one produced by beta and gamma rays emitted by radioactive isotopes. In order to reach a signal to noise ratio of the order of one, the ^{238}U and ^{232}Th content must be reduced to a level of $10^{-16}g(U)/g$ corresponding to about one count per day (cpd) in 100 tonnes.

Several techniques have been applied in order to reduce the radioisotope content in the scintillator such as distillation, water extraction and nitrogen stripping [25].
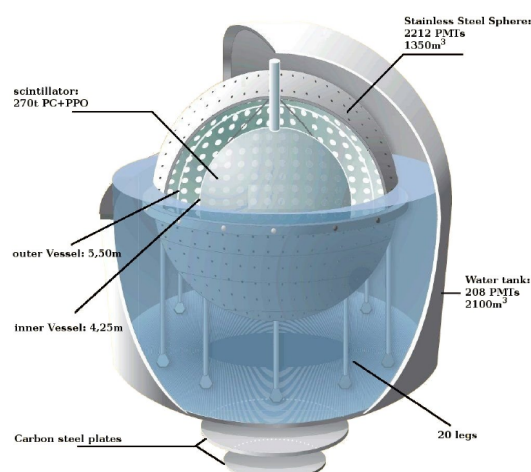
Figure 4. Sketch of the Borexino detector. The base of the dome-like structure is 18 m in diameter.

Borexino began data taking in 2007. The *PhaseI* dataset was obtained between May 2007 and May 2010. The uncertainty in the energy scale between 200 keV and 2000 keV has been determined at 1.5% precision, using multiple γ-ray sources. The position reconstruction algorithm has been tuned with the help of a *Rn* source located in 184 positions in the active volume with a steerable arm. The obtained error on the fiducial volume is (-1.3% + 0.5%).

In order to correctly model external gamma backgrounds, high energy γ-ray sources (^{208}Tl from a ^{228}Th source) were placed outside the Stainless Steel Sphere.

3. First Simultaneous Precision Spectroscopy of pp, ^{7}Be, and pep

The first simultaneous precision spectroscopy of *pp*, ^{7}Be, and *pep* is based on an exposure of 1291.51 days $\times$ 71.3 t with data collected between December 14th, 2011 to May 21st, 2016. This second phase (Borexino *PhaseII*) started after an extensive purification campaign consisting in six cycles of closed-loop water extraction, during which the radioactive contaminants were significantly reduced to: ^{238}U $< 9.4 \times 10^{-20}$ g/g (95% C.L.), ^{232}Th $< 5.7 \times 10^{-19}$ g/g (95% C.L.), ^{85}Kr, reduced by a factor ~ 4.6, and ^{210}Bi, reduced by a factor ~ 2.3

For each event, the energy, the position and the pulse shape are reconstructed by exploiting the number of detected photons and their detection times. The energy resolution is ~ 50 keV at 1 MeV. The hardware energy threshold is $N_p > 20$, (total number of triggered PMTs) which corresponds to ~ 50 keV [30]. Events are selected removing internal (external) muons [33] and applying a 300 (2) ms veto to suppress cosmogenic backgrounds. These vetos led to a total dead-time of about 1.5%.

The ^{214}Bi -^{214}Po fast coincidences from the ^{238}U chain and unphysical noise events are removed; the fraction of good events removed is $\sim 0.1\%$ and it is estimated using MonteCarlo (MC) simulations [35] and calibration data [36].

A Fiducial Volume (FV) cut is defined in order to reduce background from sources external to the scintillator in particular from the nylon vessel, from the SSS, and from PMTs. Thanks to this FV the innermost region of the scintillator is selected (71.3 t), contained within the radius $R < 2.8$ m and the vertical coordinate $-1.8 < z < 2.2$ m.

After these cuts the main background is due to radioactive isotopes in the scintillator itself: ^{14}C (β^- decay, Q = 156 keV), ^{210}Po (α decay, E = 5.3 MeV quenched by a factor ~ 10), ^{85}Kr (β^- decay, Q = 687 keV), and ^{210}Bi (β^- decay, Q = 1160 keV) from ^{210}Pb. An additional background is also due to the pile-up of uncorrelated events coming mostly from ^{14}C, external background, and ^{210}Po [34,35]. Other important contributions to the background are the residual external background, mainly due to γ's from the decay of ^{208}Tl, ^{214}Bi, and ^{40}K and the cosmogenic isotope ^{11}C (β^+ decay, $\tau = 29.4$ min)

147 that is continuously produced by muons through spallation on ^{12}C. The Collaboration has developed
148 a method called Three-Fold Coincidence (TFC) by which it it possible to tag events correlated in space
149 and time with a muon and a neutron (^{11}C is often produced together with one or even a burst of
150 neutrons). Furthermore, in order to better disentangle ^{11}C events, a e^+/e^- pulse-shape discrimination
151 is applied [30,32]. The TFC algorithm has $(92 \pm 4)\%$ ^{11}C-tagging efficiency.

152   In order to extract the interaction rates of the solar neutrinos and the background species we
153 maximize a binned likelihood function (through a multivariate approach) built as the product of 4
154 different factors; the TFC-subtracted energy spectrum, the TFC-tagged energy spectrum, the PS-$\mathcal{L}_{PR}$
155 and the radial distributions of the events.

156   In the fit procedure the neutrinos signal and the background reference spectral shapes are obtained
157 with two complementary strategies; a first one based on the analytical description of the detector
158 response function, and a second one fully based on MC simulations.

159   The interaction rates of pp, ^{7}Be, and pep neutrinos are obtained from the fit together with the
160 decay rates of ^{85}Kr, ^{210}Po, ^{210}Bi, ^{11}C, and external backgrounds due to γ rays from ^{208}Tl, ^{214}Bi, and ^{40}K.

161   Because the degeneracy between the CNO ν and the ^{210}Bi spectral shapes we have constrained
162 the CNO ν interaction rate to the HZ-SSM predictions, including MSW-LMA oscillations to 4.92 ± 0.55
163 cpd/100 t [4] [26], (3.52 ± 0.37 cpd/100 t in case of LZ-SSM). The contribution of ^{8}B ν's has been fixed
164 to the HZ-metallicity rate 0.46 cpd/100 t.

165   The ^{7}Be solar ν flux is the sum of the two mono-energetic lines at 384 and 862 keV. The uncertainty
166 in this flux has been reduced by the greatest amount.

167   To extract the pep neutrino flux we constrain the CNO one. With our sensitivity the ^{7}Be and pp ν
168 interaction rates are not affected by the hypothesis on CNO (i.e. ν's HZ hypothesis vs LZ hypothesis).
169 However, the pep ν interaction rate depends on it, being 0.22 cpd/100 t higher if the LZ hypothesis is
170 assumed.

171   The absence of the pep reaction is rejected for both the HZ and LZ assumptions with high
172 confidence in this new analysis.

173   The e^- recoil spectrum induced by CNO neutrinos and the ^{210}Bi spectrum are degenerate and
174 this makes impossible to disentangle the two contributions with the spectral fit. Due to this spectrum
175 degeneracy, it is only possible to provide an upper limit on the CNO neutrinos contribution, and
176 in order to extract this number, we have further to break the correlation between the CNO and pep
177 contributions. We exploit the theoretically well known pp and pep flux ratio in order to indirectly
178 constraint the pep ν's contribution.

179   It is possible to combine the Borexino results on pp and ^{7}Be ν fluxes in order to measure
180 experimentally the ratio $\mathcal{R}$ between the rates of the ^{3}He-^{4}He and the ^{3}He-^{3}He reactions occurring
181 within the pp chain [27]. The value of $\mathcal{R}$ tell us the competition between the two primary
182 modes of terminating the pp chain and for this reason represent a valuable probe of solar fusion.
183 In first approximation we can neglect the pep and ^{8}B ν contribution and $\mathcal{R}$ can be written as
184 $2\,\Phi(^7\text{Be})/[\Phi(\text{pp})-\Phi(^7\text{Be})]$. The measured value is in agreement with the predicted values for
185 $\mathcal{R} = 0.180 \pm 0.011$ (HZ) and 0.161 ± 0.010 (LZ) [4].

4. Improved measurement of ^{8}B solar neutrinos with 1.5 kt·y exposure

187   Concerning the ^{8}B analysis the energy threshold is set at 1650 p.e., which correspond to 3.2 MeV
188 electron energy. The analysis is based on data collected between January 2008 and December 2016 and
189 corresponds to 2062.4 live days of data. Data collected during detector operations such as scintillator
190 purification and calibrations are omitted. The dataset is split into a low energy range (LE), with [1650,
191 2950] p.e., including events from natural radioactivity, and a high energy range (HE), with [2950, 8500]
192 p.e.. This high energy region is dominated by external γ-rays following neutron capture processes
193 on the SSS. Results from the HE sample use data from the entire active volume, while the LE sample
194 requires a spatial cut to remove the top layer of scintillator (the motivation is due to the presence of
195 PPO from the scintillator leak in the upper buffer fluid volume).

196   The High Energy data sample is fitted with only two components, the ^{8}B neutrinos and the
197   external component from neutron captures, while the Low Energy sample requires three additional
198   fit components, all due to ^{208}Tl that is present in the bulk dissolved in the scintillator, at the surface
199   intrinsic to the nylon vessel, and from emanation diffused from the nylon vessel into the outer edge of
200   scintillator.

201   5. P_{ee} and ^{7}Be and ^{8}B ν reduced fluxes

202   We can write the electron neutrino survival probability as function of the neutrino energy. The
203   value for flavor conversion parameters from the MSW-LMA solution are (Δm^2_{12}=7.50×10^{-5} eV^2,
204    $\tan^2\theta_{12}$=0.441, and $\tan^2\theta_{13}$=0.022 [31]). For the ^{8}B neutrino source both the high-Z B16(GS98) SSM and
205   the low-Z B16(AGSS09met) SSM are assumed [4,7,28]. Dots represent the Borexino results from pp
206   (red), ^{7}Be (blue), pep (azure), ^{8}B neutrino measurements are in black for the LE+HE range, and grey
207   for the separate sub-ranges. For the non mono-energetic pp and ^{8}B dots are set at the mean energy of
208   detected neutrinos, weighted on the detection range in electron recoil energy. The error bars include
209   experimental and theoretical uncertainties

210   6. Toward the measurement of CNO solar neutrinos

211   CNO neutrinos have never been directly detected; according to astrophysical models, the CNO
212   cycle is responsible for about 1% of the solar neutrino luminosity and it is the main mechanism of
213   energy generation in massive stars. The Borexino Collaboration has recently concentrated all its
214   activities on the investigation of the CNO flux, the only remaining component of the solar neutrino
215   flux which has not yet been measured. The measurement of CNO neutrinos will allow to complete the
216   SSM and could solve for the Solar Metallicity Problem.
217   The measurement of the CNO flux is very challenging because the low rate expected in Borexino
218   (about 5 cpd/100t for the high metallicity or about 2 cpd/100t for the low metallicity) and it is almost
219   degenerate with the ^{210}Bi beta spectrum. Furthermore it is on the same region of the *pep* νs (but the
220   correlation *pp-pep* can help).
221   In order to extract the CNO ν signal the strategy identified by the Collaboration stands on two
222   approaches. The first one exploits the link between ^{210}Bi and ^{210}Po in order to determine the level
223   of ^{210}Bi with the required precision, while a second one would consist in an another purification
224   campaign of the scintillator, in order to further reduce the ^{210}Bi content.
225   Since the end of 2015, the detector is surrounded by a thick layer of rock wool and the dome of
226   Borexino is equipped with a water coil able to provide heat to compensate the seasonal heat exchanges
227   with the surrounding environment that have been seen to trigger fluid mixing in the IV scintillator
228   and, with it, out-of-equilibrium ^{210}Po migration towards the FV.
229   Thank to these measures the thermal stabilization of the scintillator is close to being achieved.
230   The upper part of the IV shows stable, low background levels with the ^{210}Po decay rate following a
231   nearly exponential behavior.
232   A thermally stable scintillator would allow to follow the ^{210}Po decay and, from this, to constrain
233   the ^{210}Bi rate to a precision level that would consequently allow for attempting the measurement of
234   the CNO neutrino flux.

235   7. Conclusions

236   In this talk I reported the measurements of the first complete study of the solar *pp*-chain and of its
237   different terminations by means of neutrino detection in the Borexino detector with a uniform data
238   analysis procedure.
239   Thanks to these measurements it is possible to probe our understanding of solar physics assuming
240   the validity of the neutrino oscillation mechanism or, alternatively, to test the MSW-LMA paradigm
241   assuming Standard Solar Model flux predictions.

242   The Borexino detector provides the most precise measurement of the P_{ee} survival probability
243 in the low-energy region, where flavor conversion took place in vacuum. The results obtained by
244 Borexino for the P_{ee} survival probability at higher energy, where flavor conversion is dominated by
245 matter effects, are in good agreement with the SuperKamiokande and SNO measurements.

246   I also presented the derivation for the first time of the ratio $\mathcal{R}$ between the ^{3}He-^{4}He and the
247 ^{3}He-^{3}He fusion rates. The value obtained is in agreement with the most up-to-date predicted values
248 by the SSM.

249   The results obtained by Borexino are compatible with the predictions of both high Z and low Z of
250 the SSM. However, the ^{7}Be and ^{8}B solar neutrino fluxes measured by Borexino provide an interesting
251 hint in favor of the high metallicity SSM.

252   The next goal of the Borexino Collaboration is to attempt the measurement of the, never been
253 detected, CNO neutrinos.

Acknowledgements

References

260   1.   W. A. Fowler, The Astrophysical Journal **127**, 551, (1958)
261   2.   A. W. G. Cameron, Annual Review of Nuclear Science, **8**, 299, (1958)
262   3.   J. N. Bahcall and M. H. Pinsonneault, Phys. Rev. Lett. **92**, 121301 ,(2004).
263   4.   N. Vinyoles, A. M. Serenelli, F. L. Villante, S. Basu, J. Bergström, M. C. Gonzalez-Garcia, M. Maltoni, C.
264   Peña-Garay, and N. Song, The Astrophysical Journal **835**, 202 (2017).
265   5.   N. Grevesse and A. J. Sauval, Space Sci. Rev. **85**, 161 (1998).
266   6.   M. Asplund, N. Grevesse and J. Sauval, Nucl. Phys. A **777**, 1 (2006)
267   7.   M. Asplund, N. Grevesse, A. J. Sauval, and P. Scott, Ann. Rev. Astron. Astrophys. **47**, 481 (2009),
268   8.   A. Serenelli, S. Basu, J. W. Ferguson and M. Asplund, Astrophys. J. **705**, L123 (2009)
269   9.   J. N. Bahcall, Phys. Rev. Lett. **12**, 300 (1964).
270   10.   R. J. Davis, Phys. Rev. Lett. **12**, 302 (1964).
271   11.   R. J. Davis, D. S. Harmer and K. C. Hoffman, Phys. Rev. Lett. **20**, 1205 (1968).
272   12.   B. T. Cleveland, The Astrophysical Journal, **496**, 505 (1998)
273   13.   K. S. Hirata *et al.*, Phys. Rev. Lett. **63**, 16 (1989).
274   14.   Y. Fukuda *et al.*, Phys. Rev. Lett. **82**, 2430 (1999) .
275   15.   J.N. Abdurashitov et al., Phys. Rev. Lett. **83**, 4686 (1999).
276   16.   W. Hampel et al., Phys. Lett. B **447**, 127 (1999).
277   17.   M. Altmann et al., Phys. Lett. B **616**, 174 (2005).
278   18.   L. Miramonti and F. Reseghetti, Riv. Nuovo Cim. **25**, N7 (2002).
279   19.   Q. R. Ahmad *et al.*, Phys. Rev. Lett. **87**, 071301 (2001).
280   20.   Q. R. Ahmad *et al.*, Phys. Rev. Lett. **89**, 011301 (2002).
281   21.   S. N. Ahmed *et al.*, Phys. Rev. Lett. **92**, 181301 (2004).
282   22.   L. Wolfenstein, Phys. Rev. D **17**, 2369 (1978).
283   23.   S. P. Mikheev and A. Y. Smirnov, Sov. J. Nucl. Phys. **42**, 913 (1985)
284   24.   G. Alimonti *et al.*, NIM A **600**, 568 (2009).
285   25.   G. Alimonti *et al.*, NIM A **609**, 58 (2009).
286   26.   I. Esteban *et al.* Journal of High Energy Physics **01**, (2017)
287   27.   C. Peña-Garay, Journal of High Energy Physics **11** (2003)
288   28.   N. Grevesse and A. Sauval, Space Science Reviews 85, **161** (1998).
289   29.   G. Bellini *et al.* Physical Review Letters **107**, 141302 (2011)
290   30.   G. Bellini *et al.* Physical Review D **89**, 112007 (2014)

291   31.   I. Esteban, M. C. Gonzalez-Garcia, M. Maltoni, I. Martinez-Soler, and T. Schwetz, JHEP **01**, 087 (2017)
292   32.   G. Bellini *et al.* Physical Review Letters **108**, 051302 (2012)
293   33.   G. Bellini *et al.* Journal of Instrumentation **6**, P05005 (2011)
294   34.   G. Bellini *et al.* Nature **512**, 383 (2014)
295   35.   M. Agostini *et al.* Astroparticle Physics **97**, 136 (2017)
296   36.   H. Back *et al.* Journal of Instrumentation **7**, P10018 (2012)
297   37.   M.Agostini *et al.* arXiv:1709.00756v1 [hep-ex]
298   38.   M.Agostini *et al.* arXiv:1707.09278v2 [hep-ex]